Preparation and properties of Co$_{0.85}$Se/RGO composite counter electrodes for quantum-dot-sensitized solar cells

MAOLIN ZHANG [a,*,] JING LI [a], ZHIQIANG NIE[b,*], DONGYAN ZHANG[a,] YANGXI YAN[a], ZHIMIN LI[a]
aSchool of Advanced Materials and Nanotechnology, Xidian University, Xi'an, 710071, China
bXi'an Institute of Optics and Precision Mechanics, Chinese Academy of Sciences, Xi'an, 710119, China

Counter electrodes (CEs) are fundamentally important components of quantum-dot-sensitized solar cells (QDSSCs), helping to transfer electrons from external circuit to electrolyte and acting as catalysts. In this work, Co$_{0.85}$Se/RGO composite films were synthesized via one-step solvothermal process. X-ray diffraction (XRD), scanning electron microscope (SEM) and energy-dispersive spectrometer (EDS) were utilized to characterize the structure, morphology and elemental distribution of the composite CEs. The photovoltaic studies revealed that the composite CEs could yield PCE reaching 2.6% when assembled with CdS/CdSe/TiO$_2$ photoanodes for QDSSCs. EIS and Tafel polarization indicated that the enhanced performances were due to combined high catalytic properties of Co$_{0.85}$Se with better electron conductivity of RGO.

1. Introduction

Solar radiation is a clean power that can be converted into electrical and thermal energy [1]. Quantum dot sensitized solar cells (QDSSCs) have attracted considerable attention due to their superior high theoretical power conversion efficiency (44%), convenient preparation processes, and low-cost [2]. Basically, QDSSCs consist of photoanode, electrolyte and counter electrode (CE) assembled in sandwich-like structures [3]. CEs play essential roles in electron transfer and catalysis in QDSSCs to promote the reduction of the electrolyte [4]. Hence, CEs with high electrical conductivities and catalytic properties would enhance the power conversion efficiency (PCE) of QDSSCs. Moreover, ideal CEs should possess relevant chemical stability with high resistance to both corrosion and solubility [5-7].

Metal selenides CEs like PbSe and Cu$_{2-x}$Se have excellent photovoltaic performances reaching 4.7% for PbSe and 6.25% for Cu$_{2-x}$Se [4, 8]. Hou et al. reported two-dimensional cobalt selenide with outstanding conductivity and catalytic activity owing to overlapped Co 3d and Se 4p electrons [9]. Accordingly, cobalt selenides have successfully been applied as catalysts with tremendous electrochemical performances, reusability, and catalytic activities [10-11]. Wu et al. synthesized folded nanosheet-like Co$_{0.85}$Se arrays with superior durability and high activity [12]. Cobalt selenides were firstly used as CEs for DSSCs with high PCE reaching 9.4% [13]. However, CoSe$_2$ which employed as CE for QDSSCs induced only a PCE of 1.85% [4]. A bifacial QDSSC was then prepared using Co$_{0.85}$Se as CE by mild hydrothermal route with slightly improved PCE of 2.1% [14]. Co$_{0.85}$Se films were also prepared by a one-step solvothermal method with improved electrochemical performances in our previous work [15]. However, the obtained PCE for QDSSCs assembled with Co$_{0.85}$Se CE and CdS/CdSe co-sensitized photoanodes still moderate and require improvement.

Composite materials have widely been applied as CEs for QDSSCs to combine the merits of individual components for optimized performances. In generally, CEs consist of materials with superior catalytic activities and high electrical conductivities. Hence, the combination of metal selenide/sulfide catalysts (such as CuS, PbSe, and CoSe) together with conductive carbon materials (such as reduced graphene oxide (RGO), carbon nanotubes, and activated carbon) should lead to high-performance CEs. For instance, CoS$_2$-CoSe$_2$/N-doped carbon composite CEs have been successfully prepared for DSSCs with PCE reaching 8.45% [16]. DSSCs assembled with Co$_{0.85}$Se nanotube/RGO composite CEs exhibited a remarkable PCE of 7.81% [17]. Cu$_2$S/RGO composites were synthesized by facile solvothermal with enhanced electrocatalytic performances, good stability, and high PCE of 3.85% for QDSSCs [18].

In this work, Co$_{0.85}$Se/RGO composite materials were deposited on FTO substrates by one-step solvothermal route to integrate the advantages of both materials. The structures, morphologies, elemental distribution and electrochemical properties of the obtained composite CEs were studied. The photovoltaic performances of assembled QDSSCs with the obtained composite CEs and CdS/CdSe co-sensitized photoanodes were also evaluated and the results were discussed.

2. Experimental

2.1. Preparation of CEs

CEs were prepared by the solvothermal method. Firstly, reduced graphene oxide (RGO) was obtained by improved Hummer method using graphite powder as raw material [19]. $CoCl_2$ (AR, Sinopharm Group) and Na_2SeO_3 (AR, Josiah Reagent) at molar ratio of 1:1.2 were then dissolved in ethylene glycol as reagents. Next, RGO was added to the solution at different weight ratios of $CoCl_2$ to RGO. A cleaned FTO with conductive layer heading down was placed in a polytetrafluoroethylene autoclave. The mixed solution was then poured into the autoclave to completely immerse the FTO. The $Co_{0.85}Se$/RGO CE film was obtained after treatment of the autoclave at 180 ℃ for 12 h, and the resulting composite CEs were denoted as Co/RGO0.05, Co/RGO0.1, Co/RGO0.5 and Co/RGO0.75 for reactant mass ratios of $CoCl_2$ and RGO of 1:0.05, 1:0.1, 1:0.5 and 1:0.75, respectively. The CEs without composites were named as $Co_{0.85}Se$ and RGO.

2.2. Cell assembly

The mesoporous TiO_2 films sensitized by CdS/CdSe QDs through successive ionic layer adsorption and reaction (SILAR) followed by chemical bath deposition (CBD) methods were employed as photoanodes [3, 20]. The active area of this device was about 0.2 cm^2. A polysulfide containing 1 M S and 1 M Na_2S in deionized water was used as electrolyte. The QDSSCs cells were assembled by sandwiching the prepared composite CE, photoanode and polysulfide electrolyte [21-22].

2.3. Characterization

X-ray diffraction (XRD, D8 Advance, Bruker, Germany) with Cu Kα radiation (λ=0.15418 nm) was used to characterize the phase structure of prepared composite CEs. The XRD were acquired over a 2θ range of 15°~80° with a step of 0.02°. Field emission scanning electron microscope (FESEM, JSM-7500F, JEOL, Japan) was applied to investigate the morphology. Energy-dispersive spectrometer (EDS, X-Max50, Oxford, England) was used to observe the element distribution. Electrochemical impedance spectra (EIS) and Tafel polarization were carried out by electrochemical workstation (CHI660E, Chinstruments, China) to explore the electrochemical performances of CEs. The photovoltaic properties of QDSSCs were measured using a photoelectrochemical system (Zahner, CIMPS-II, Germany) under AM 1.5 simulated sunlight with a power density of 100 mW/cm^2.

3. Results and discussion

3.1. Phase structure and morphology

XRD was used to confirm phase structures of the prepared CEs and the data are gathered in Fig. 1. Three intensive peaks at 2θ=33.5°, 45.1° and 51.0° were observed, corresponding to the crystal plane of (101), (102) and (110), respectively. This indicated the successful preparation of $Co_{0.85}Se$ with hexagonal structure [15]. On the other hand, a broad diffraction peak appeared at 2θ=23.6°, assigned to the (002) crystal plane of graphene. The intensity of this peak increased with added RGO. In sum, these data confirmed the successful preparation of $Co_{0.85}Se$/RGO composites.

SEM combined with EDS mapping was used to analyze the morphology and elemental distribution of the prepared composites. As shown in Fig. 2(A), RGO showed a porous sheet structure with many adhering sites for $Co_{0.85}Se$ loading. $Co_{0.85}Se$ particles with different morphologies and sizes successfully adhered on the graphene surface. According to our previous work [15], $Co_{0.85}Se$ particles prepared by solvothermal method had irregularly spherical shapes. At very low initial reactant concentration of graphene (Co/RGO0.05), $Co_{0.85}Se$ particles accumulated on the graphene surface since RGO did not provide enough adhesion growth interfaces. As RGO concentration increased, appropriate amount of graphene provided suitable amounts of active points for $Co_{0.85}Se$. Therefore, $Co_{0.85}Se$ particles uniformly grew and distributed on the graphene sheet with particle diameter around 300 nm (Fig. 2 (C)).
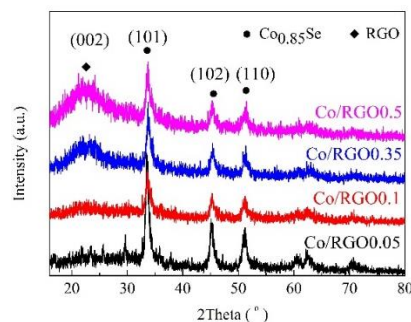

Fig. 1. XRD profiles of prepared $Co_{0.85}Se$/RGO composite CEs

(color online)

The EDS mapping of Co/RGO0.1 is shown in Fig. 3. C was derived from graphene, both Co and Se came from $Co_{0.85}Se$ particles grown on the graphene sheet layers. Also, C, Co and Se looked uniformly distributed on the surface, indicating the uniform distribution of cobalt selenide particles on the graphene multi-layer sheets. As graphene amount further rose, it provided sufficient adhesion interfaces to allow nucleation of $Co_{0.85}Se$. This resulted in very small $Co_{0.85}Se$ particles dispersed in the graphene sheet (Fig. 2(D)).

3.2. Electrochemical and photovoltaic performances

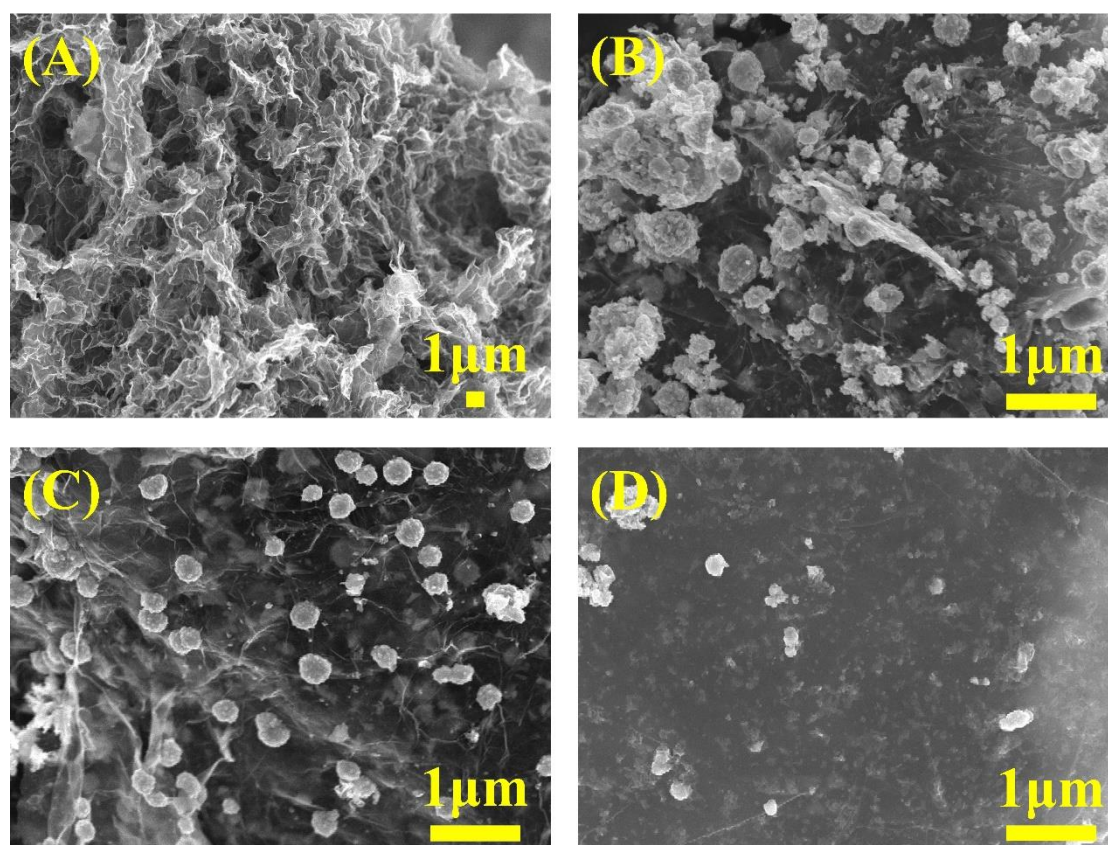EIS and Tafel polarization were utilized to investigate

Fig. 2. SEM images of different counter electrode materials: (A) RGO, (B) Co/RGO0.05, (C) Co/RGO0.1, and (D) Co/RGO0.5
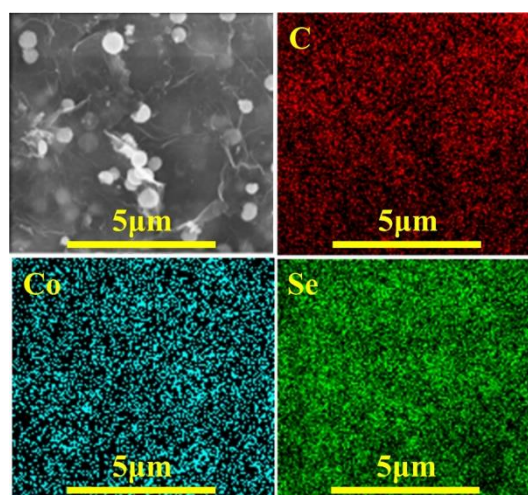
Fig. 3. EDS mapping of Co/RGO0.1 (color online)

The electrocatalytic performances of Co$_{0.85}$Se/RGO composite electrodes and the data are displayed in Fig. 4. EIS measurements were performed using symmetric cells made of two identical counter electrodes (CE/electrolyte/CE). A Z-view software was used to fit the test data and the parameters are listed in Table 1. The equivalent circuit revealed synergy of series resistance (R$_s$), charge transfer resistance (R$_{ct}$), Warburg diffusion impedance (Z$_w$), and chemical capacitance (C$_{PE}$) at the interface between the counter and electrolyte [23-25]. The R$_s$ values of Co$_{0.85}$Se/RGO composite electrodes looked obviously lower than those of Co$_{0.85}$Se electrodes thanks to the good conductivity of graphene. As RGO content increased, R$_s$ decreased from 10.6 to 5.1 Ω/cm^2. On the other hand, R$_s$ was associated with connectivity of the electrode film to the substrate. Co$_{0.85}$Se/RGO composites

prepared by solvothermal method grew well on the FTO substrates, leading to lower R_s values of composite electrodes when compared to RGO electrodes. R_{ct} obtained from the Nyquist curve would provide information about the electron transfer at the interface between CEs and electrolyte [26]. CEs with lower R_{ct} would have higher catalytic activities. R_{ct} of composite CEs were much lower than those of $Co_{0.85}Se$, indicating better electrocatalytic activities of composite CEs. On the other hand, Co/RGO0.1 showed the lowest R_{ct} (0.19 Ω/cm^2) among all composite CEs, meaning that $Co_{0.85}Se$ particles uniformly distributed on the graphene with homogeneous size could effectively enhance the reaction between the electrolyte and counter electrode. The graphene facilitated the electron transfer to $Co_{0.85}Se$. Therefore, Co/RGO0.1 electrode could quickly catalyze the reduction reaction of S_n^{2-} in the electrolyte.

Tafel polarization tests were used to further analyze the catalytic performances of the composite counter electrodes and the results are displayed in Fig. 4(B). In the Tafel polarization curves, the exchange current density (J_0) and R_{ct} were inversely proportional to each other. This might exemplify the catalytic activities of CEs. The relationship

between J_0 and R_{ct} can be expressed following Eq. (1),

$$J_0 = \frac{RT}{nFR_{ct}} \tag{1}$$

where R, T, n and F represent for the gas constant, temperature, number of effective electrons contributing to charge transfer at the interface and the Faraday constant, respectively.

The largest J_0 (3.85 mA/cm^2) was obtained using Co/RGO0.1, indicating its good catalytic activity and fast charge transfer rate at the CE/electrolyte interface. The changing trend of J_0 was well consistent with that of R_{ct} in EIS profiles. On the other hand, the limiting current density (J_{lim}) was directly associated with diffusion of S^{2-}/S_n^{2-} redox couple obtained by diffusion of carriers at the CE/electrolyte interface [23, 25, 27]. In Eq. (2), the large J_{lim} in Tafel curve indicated high diffusion coefficient (D) and fast diffusion velocity in the polysulfide electrolyte [25, 27].

Table 1. Electrochemical parameters of different CEs

Sample	$Co_{0.85}Se$	RGO	Co/RGO0.05	Co/RGO0.1	Co/RGO0.5	Co/RGO0.75
Rs(Ω/cm^2)	19.7	5.9	10.6	5.6	5.1	5.4
Rct(Ω/cm^2)	19.4	0.20	0.39	0.19	0.25	0.59

$$D = \frac{lJ_{lim}}{2nFC} \tag{2}$$

where l and C are the distance between two electrodes and S_n^{2-} concentration, respectively.

The J_{lim} of Co/RGO0.1 was estimated to 177.83

mA/cm^2, and notably higher than those of other CEs. This indicated rapid diffusion velocities at the CE/electrolyte interface and better utilization of electrons to reduce S_n^{2-}. In turn, these features led to enhanced catalytic activities of the CEs.

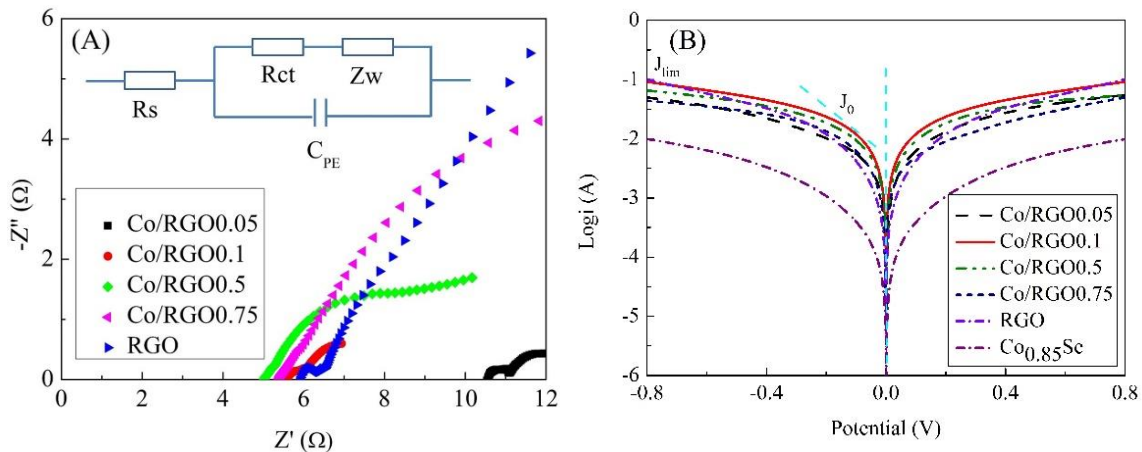*Fig. 4. Electrochemical properties of different CEs, EIS (A), and Tafel polarization curves (B) (color online)*

The prepared $Co_{0.85}Se$/RGO CEs were assembled with CdS/CdSe co-sensitized TiO$_2$ photoanodes in S^{2-}/S_n^{2-} electrolyte to yield QDSSCs cells. The J-V characteristics

of the cells and typical photovoltaic parameters are illustrated in Figure 5 and Table 2. The V_{oc} values of QDSSCs fabricated with different composite CEs looked

close to each other (0.53~0.56 V) but were much higher than that of pure Co$_{0.85}$Se counter electrode. This was attributed to the good electrical conductivity of graphene, which effectively enhanced the charge transport process.

J$_{sc}$ was also improved when compared to pure graphene CE, indicating that Co$_{0.85}$Se particles grown on the graphene surface rapidly catalyzed the oxidation of the electrolyte and improved the charge transport rate. The fill factor (FF) was mainly related to the internal resistance of cells. When combined with EIS data, the R$_{ct}$ (0.19 Ω/cm^2) of Co$_{0.85}$Se/graphene composite CEs appeared significantly smaller than that of Co$_{0.85}$Se CE (19.4 Ω/cm^2). For Co$_{0.85}$Se/graphene composite CEs, the Co$_{0.85}$Se particles uniformly and homogeneous distributed on the surface led to an increase in contact between the electrolyte and CE. The graphene facilitated the electron transfer to the Co$_{0.85}$Se particles, catalytically reducing Sn^{2-} in the electrolyte so that cycling process in QDSSC could complete promptly. Therefore, the composite counter electrodes in contact with S^{2-}/S$_n^{2-}$ electrolyte might effectively reduce the internal recombination process of QDSSCs, thereby improving the FF and J$_{sc}$. The best performance was obtained at mass ratio of Co$_{0.85}$Se to graphene of 1:0.1, with PCE reaching 2.6% (J$_{sc}$ = 9.7 mA/cm^2, FF = 47.9%, and V$_{oc}$ = 0.56 V).
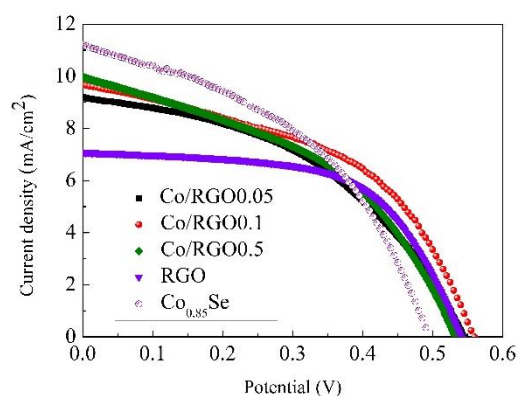

Fig. 5. Current density-voltage (J-V) curves of different QDSSCs assembled with CdS/CdSe co-sensitized TiO$_2$ photoanode, S^{2-}/S$_n^{2-}$ electrolyte, and different counter electrodes (color online)

However, PCE in this work is still very low compared with theoretical value. One of the reasons is that the TiO$_2$ photoanode is merely sensitized by CdS/CdSe quantum dots. On the other hand, the electrocatalytic activity and electrical conductivity of the CEs need further enhancements. Therefore, novel effective quantum dots and newly developed CEs with high electrocatalytic activity and excellent electrical conductivity are the primary approaches to improving the performances of photoelectric characteristics.

Table 2. Photoelectric performances of QDSSCs assembled by CdS/CdSe co-sensitized TiO$_2$ photoanode, S^{2-}/S$_n^{2-}$ electrolyte, and different counter electrodes

Sample	J$_{SC}$ (mA/cm^2)	V$_{OC}$ (V)	FF (%)	η (%)
Co/RGO0.05	9.17	0.54	44.70	2.2
Co/RGO0.1	9.69	0.56	47.94	2.6
Co/RGO0.5	9.95	0.53	43.45	2.3
Co$_{0.85}$Se	11.2	0.50	42.9	2.4
RGO	7.08	0.54	59.64	2.3

4. Conclusions

Co$_{0.85}$Se/RGO composite film counter electrodes were successfully prepared on FTO substrates by one-step solvothermal process. The suitable mass ratios of Co$_{0.85}$Se to RGO led to the formation of composite materials with uniform distribution of Co$_{0.85}$Se particles. The EIS and Tafel polarization tests indicated that RGO can facilitate the electron transfer from the external circuit to Co$_{0.85}$Se particles followed by reduction of S$_n^{2-}$ in the electrolyte by Co$_{0.85}$Se to quickly complete the internal circulation process of QDSSCs. The best performance of QDSSCs was obtained at mass ratio of Co$_{0.85}$Se to RGO of 1:0.1, with PCE reaching 2.6% (J$_{sc}$ = 9.7 mA/cm^2, FF = 47.9%, and V$_{oc}$ = 0.56 V).

References

[1] S. Rühle, M. Shalom, A. Zaban. Chem. Phys. Chem. **11**, 2290 (2010).
[2] J. K. Sun, Y. Jiang, X. H. Zhong, J. S. Hu, L. J. Wan, Nano Energy **32**, 130 (2017).

[3] M. D. Ye, X. Y. Gao, X. D. Hong, Q. Liu, C. F. He, X. Y. Liu, C. J. Lin, Sustain. Energ. Fuels. **1**, 1217 (2017).

[4] H. M. Choi, I. A. Ji, J. H. Bang, ACS Appl. Mater. Inter. **6**, 2335 (2014).

[5] G. Zhu, L. K. Pan, T. Xu, Z. Sun, ACS Appl. Mater. Inter. **3**, 3146 (2011).

[6] J. L. Duan, H. H. Zhang, Q. W. Tang, B. L. He, L. M. Yu, J. Mater. Chem. A **3**, (2015) 34.

[7] V. Chakrapani, D. Baker, P. V. Kama, J. Am. Chem. Soc. **133**, 9607 (2011).

[8] X. Q. Chen, Z. Li, Y. Bai, Q. Sun, L. Z. Wang, S. X. Dou, Chem.-Eur. J. **21**, 1055 (2015).

[9] Y. Hou, M. R. Lohe, J. Zhang, S. H. Liu, X. D. Zhuang, X. L. Feng, Energ. Environ. Sci. **9**, 478 (2015).

[10] T. Chen, S. Z. Li, J. Wen, P. B. Gui, G. J. Fang, ACS Appl. Mater. Inter. **9**, 35927 (2017).

[11] C. C. Liu, J. M. Song, J. F. Zhao, H. J. Li, H. S. Qian, H. L. Niu, C. J. Mao, S. Y. Zhang, Y. H. Shen, Appl. Catal. B-Environ. **119**, 139 (2012).

[12] Z. C. Wu, J. J. Li, Z. X. Zou, X. Wang., J. Solid. State. Electr. **22**, 1785 (2018).

[13] F. Gong, H. Wang, X. Xu, G. Zhou, Z. S. Wang, J. Am. Chem. Soc. **134**, 10953 (2012).

[14] C. Q. Ma, Q. W. Tang, Z. Y. Zhao, M. J. Hou, Y. R. Chen, B. L. He, L. M. Yu, J. Power. Sources **278**, 183 (2015).

[15] X. Ji, M. L. Zhang, D. Y. Zhang, Y. Wang, Y. X. Huang, Y. X. Yan, P. Sun, Z. M. Li, J. Nanosci. Nanotechno. **19**, 5338 (2019).

[16] S. S. Huang, H. T. Wang, S. D. Wang, Z. J. Hu, L. Zhou, Z. W. Chen, Y. Jiang, X. F. Qian, Dalton. T. **47**, 5236 (2018).

[17] H. Yuan, Q. Z. Jiao, J. Liu, X. F. Liu, Y. J. Li, D. X. Shi, Q. Wu, Y. Zhao, H. S. Li, Carbon **122**, 381 (2017).

[18] M. D. Ye, C. Chen, N. Zhang, X. R. Wen, W. X. Guo, C. J. Lin, Adv. Energy. Mater. **4**, 1301564 (2014).

[19] X. Ji, M. L. Zhang, P. Zhong, D. Y. Zhang, P. Sun, Y. Wang, Z. M. Li, Optoelectron. Adv. Mat. **13**(5-6), 348 (2019).

[20] J. Kusuma, R. G. Balakrishna, Sol. Energy. **159**, 682 (2018).

[21] Y. Li, L. L. Zhao, Z. L. Du, J. Du, W. Wang, Y. Wang, L. J. Zhao, X. M. Cao, X. H. Zhong, J. Mater. Chem. A **6**, 2129 (2018).

[22] M. Samadpour, S. Arabzade, J. Alloy. Compd. **696**, 369 (2017).

[23] Y. Bai, C. Han, X. Q. Chen, H.Yu, X. Zong, Z. Li, L. Z. Wang, Nano Energy **13**, 609 (2015).

[24] Gopi Chandu, V. V. Muralee, M. Venkata-Haritha, K. Soo-Kyoung, R. S. Srinivasa, P. Dinah, K. Hee-Je, RSC Adv. **5**, 2963 (2015).

[25] Gopi Chandu, V. V. Muralee, S. Saurabh, R. A. Eswar, K. Hee-Je, ACS Appl. Mater. Inter. **10**, 10036 (2018).

[26] I. Hwang, K. Yong, Chem. Electro. Chem. **2**, 634 (2015).

[27] B. B. Jin, Y. F. Wang, X. Q. Wang, J. H. Zeng, Appl. Surf. Sci. **369**, 436 (2016).

———————————————————
*Corresponding authors: mlzhang@xidian.edu.cn; niezq@opt.ac.cn